TOPICAL REVIEW

Insight into constitutive theories of 4D printed polymer materials: a review

To cite this article: Jesus A Rodriguez-Morales *et al* 2024 *Smart Mater. Struct.* **33** 073005

IOP Publishing Smart Materials and Structures
Smart Mater. Struct. **33** (2024) 073005 (20pp) https://doi.org/10.1088/1361-665X/ad523c

Topical Review

Insight into constitutive theories of 4D printed polymer materials: a review

Jesus A Rodriguez-Morales[1], Hao Duan[1], Jianping Gu[2], Hao Zeng[3,*] and Huiyu Sun[1,*]

[1] State Key Laboratory of Mechanics and Control of Mechanical Structures, Nanjing University of Aeronautics and Astronautics, Nanjing, People's Republic of China
[2] Jiangsu Key Laboratory of Advanced Structural Materials and Application Technology, School of Materials Science and Engineering, Nanjing Institute of Technology, Nanjing, People's Republic of China
[3] School of Physical and Mathematical Sciences, Nanjing Tech University, Nanjing, People's Republic of China

E-mail: zenghao@njtech.edu.cn and hysun@nuaa.edu.cn

Received 5 January 2024, revised 7 May 2024
Accepted for publication 30 May 2024
Published 19 June 2024

Abstract

Four-dimensional (4D) printing has emerged as a branch of additive manufacturing that utilizes stimuli-responsive materials to generate three-dimensional structures with functional features. In this context, constitutive models play a paramount role in designing engineering structures and devices using 4D printing, as they help understand mechanical behavior and material responses to external stimuli, providing a theoretical framework for predicting and analyzing their deformation and shape-shifting capabilities. This article thoroughly discusses available constitutive models for single-printed and multi-printed materials. Later, we explore the role of machine learning (ML) algorithms in inferring constitutive relations, particularly in viscoelastic problems and, more recently, in shape memory polymers. Moreover, challenges and opportunities presented by both approaches for predicting the mechanical behavior of 4D printed polymer materials are examined. Finally, we concluded our discussion with a summary and some future perspectives expected in this field. This review aims to open a dialogue among the mechanics community to assess the limitations of analytical models and encourage the responsible use of emerging techniques, such as ML. By clarifying these aspects, we intend to advance the understanding and application of constitutive models in the rapidly growing field of 4D printing.

Keywords: 4D printing, constitutive modeling, shape memory polymers, machine learning

1. Introduction

Additive manufacturing (AM) has rapidly advanced owing to the degree of freedom and complexity that allows prototype manufacturing [1]. Since its origin in the early 1980 [2, 3], three-dimensional (3D) printing has found diverse applications in many fields, including biomedicine [4], construction [5], and engineering [6]. Shape memory polymers (SMPs) and their composites have also made significant progress and are becoming highly useful in numerous applications requiring specific characteristics. Their advantages over shape memory alloys include lower cost, lower density, better deformation recovery, biodegradability, and

* Authors to whom any correspondence should be addressed.

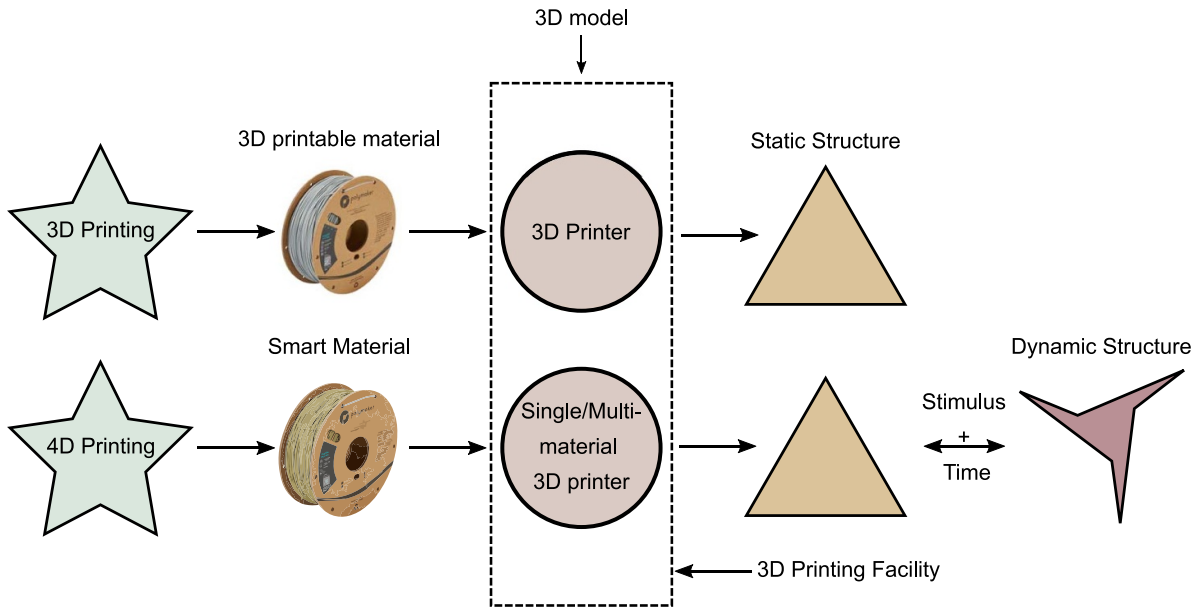

Figure 1. Schematic of the difference between 3D and 4D printing technologies.

responsiveness to a broad range of stimuli [7]. However, limitations such as low actuation rates and poor shape memory cycle times exist [8].

SMPs are highly versatile and can exist in various forms, such as films, foams, and bulk materials. Another method of manufacturing SMPs is 3D printing, which results in four-dimensional (4D) printing. It means an object is printed flat and obtains a 3D shape after exposure to external stimuli. 3D and 4D printing represent two distinct yet interrelated domains within advanced manufacturing. Although both processes involve the additive fabrication of 3D objects from digital designs, they diverge significantly in their capabilities and outcomes. While 3D printing focuses on creating static objects layer by layer, 4D printing has the capacity for those objects to transform or adapt their shape or properties over time, providing additional functionality and versatility (see figure 1).

4D printing is a growing research field with large areas yet to be explored. With applications covering multiple sectors, its unique self-morphing, self-healing, and self-actuation capabilities have opened a new manufacturing paradigm [9, 10].

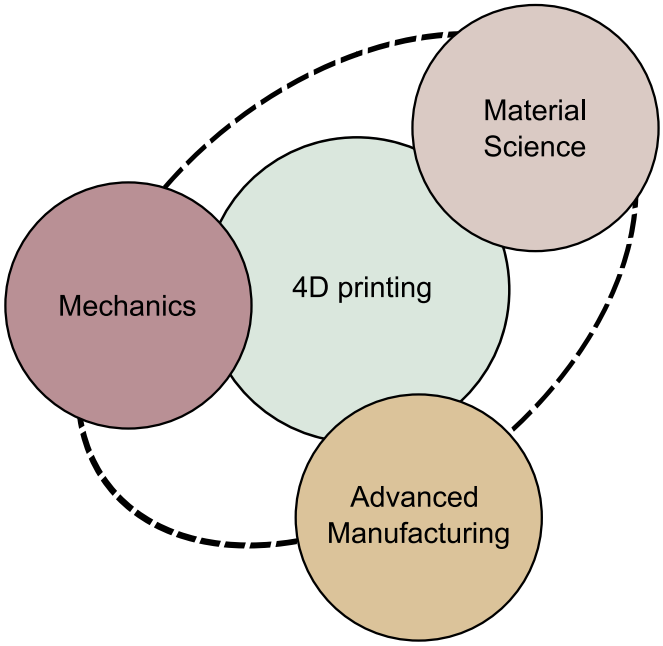

Figure 2. Disciplines integrated in 4D printing.

1.1. Significance

Since its introduction in 2013 [11], this new manufacturing method has revolutionized multiple areas (e.g. smart textiles, aerospace structures, and bioprinting) due to the printed material's capacity to evolve within a predetermined manner. In general, 4D printing relies on five factors: the material used, mechanisms of interaction, the stimulus of smart materials, printing methods, and mathematical modeling [12, 13]. Figure 2 shows the disciplines encompassing these factors.

Current reviews offer valuable insights into various aspects of 4D printing, including AM processes [14, 15], shape-changing abilities [16, 17], utilized stimuli [18, 19], applications within the biomedical sector [20–24], specific engineering fields [25–30], materials used for this technology [8, 13, 31–33], printing at small scales [34, 35], and the impact of printing parameters on material behavior [36–38]. However, as far as we know, there is no review concerning the available mathematical models for 4D printed polymer materials.

Constitutive theories play a crucial role in understanding mechanical behavior and the response of materials to external stimuli, providing a theoretical framework for predicting and analyzing their deformation and shape-shifting capabilities. However, existing reviews broadly focus on the technological aspects, applications, and materials used in 4D printing, with limited attention given to the theoretical foundations governing the material behavior. Such a review would not only bridge the existing gap in the literature but also provide valuable insights for researchers, engineers, and designers looking to exploit the adaptive capabilities of 4D printing for multiple applications.

1.2. Review's organization

In this article, we start the first section with single-printed materials, often exhibiting the shape memory effect (SME), followed by multi-printed materials that rely on the deformation mismatch to evolve. Later in our discussion, we will explore the role of machine learning (ML) algorithms inferring constitutive relations in viscoelastic problems. This strategy is becoming increasingly common for inferring parameters or constitutive laws in composite materials and, more recently, SMPs. The contributions of this study are as follows:

(i) Provide a concise yet meaningful review of the current constitutive models used in 4D printing.
(ii) Open a dialogue to assess the current limitations of existing models.
(iii) Provide enough background for new readers in the field.

2. Single-printed materials

The materials frequently used for 4D printing include thermoplastic filaments such as polylactide acid (PLA), acrylonitrile butadiene styrene (ABS), polyvinyl alcohol (PVA), and polycarbonate (PC). These materials can memorize a permanent shape and allow the recovery of this shape from a temporary one when stimulated, displaying the SME. Materials that experience the SME are commonly categorized by one, two, or triple-way SME [19] (see table 1 and figure 3). For SMPs, constitutive laws are more complex than those for common engineering materials because they rely on time and temperature, external loading, loading rate, damage status, and programming history [47].

Over the past few years, the mechanics community has obtained an initial understanding of the SME based on the development of thermomechanical theory, either with the viscoelasticity theory or the phase transition theory [48, 49]. In the literature, there are relevant reviews dealing with constitutive laws for thermo-active SMPs [50–53] and even a tutorial recently published by Yan and Li [54] where the reader can consult for further information about the classical models and how they have improved.

For 4D printed SMPs, classical models do not consider that the printing parameters affect the final material behavior and the pre-strain stored in the filaments [28, 55]. During the printing process, parameters such as nozzle temperature, layer height, printing speed, bed temperature, printing pattern and the interaction effect between them are the most common to do so [38, 56–58]. In addition, the layered manufacturing process may introduce additional porosity and anisotropy, which could negatively impact their mechanical properties [59]. Therefore, this section begins with an overview of classical models used for 4D single-printed materials. Later, we discuss the multiple efforts to link the manufacturing process conditions with the final mechanical performance of 4D printed polymers.

Table 1. Representative phenomenological models based on their SME classification.

Type of model	Material behavior	References
One-way	Hyperelastic viscoelastic visco-hyperelastic	[39–43]
Two-way	Elastoplastic hyperelastic	[28, 44]
Triple-way	Elastoplastic	[45]

2.1. Rheological models

Constitutive modeling of thermo-SMPs has a consolidated background since its introduction in 1997 when Tobushi *et al* [48] proposed the first rheological model based on the linear theory of viscoelasticity. Based on a similar framework, many other viscoelastic models have been developed to describe the large deformations of SMPs [60–62]. These models capture hysteresis from structural and stress-relaxation perspectives. However, they have been unable to relate phase transition mechanisms to SME and provide a clear physical interpretation.

For 4D printed materials, researchers have adopted existing rheological models because this technology relies on the use of SMPs. One of the usual fields of application of these models is the development of 4D cellular structures. Inspired by the unique microstructure of a porous glass sponge, Zhao *et al* [63] designed a functional tracheal scaffold. In this study, Zhao and collaborators used the generalized Maxwell model to simulate the deformation process and the neo-Hooke model to describe the deformation behavior at high temperatures. Later, Wan *et al* [64] introduced a programmable lattice metamaterial with a changing topological angle and radius, enabling adjustment of the mechanical properties. This concept proved effective by fabricating a 3D cylindrical shell subjected to tension and bending loads. The deformation process was described using a 3D multi-branch thermoviscoelastic model coupled with the Arruda–Boyce eight-chain model [65].

Liu *et al* [66] investigated the anisotropic characteristics of mechanical and shape memory performances of 4D printed PLA with infill patterns. They combined the laminate plate and honeycomb equivalent modulus theories with a generalized

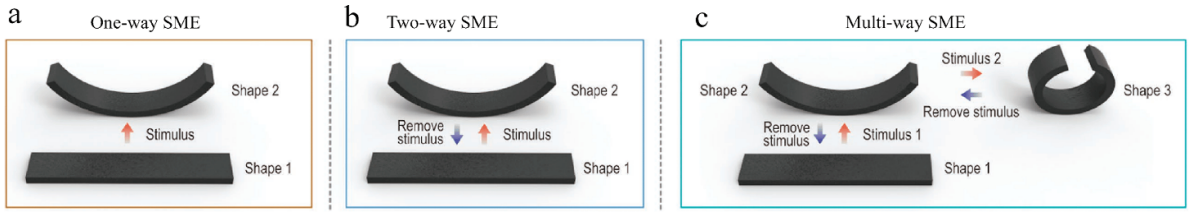

Figure 3. Schematic of shape memory effect: (a) one-way, (b) two-way, (c) multi-way. [46] John Wiley & Sons. © 2019 WILEY-VCH Verlag GmbH & Co. KGaA, Weinheim.

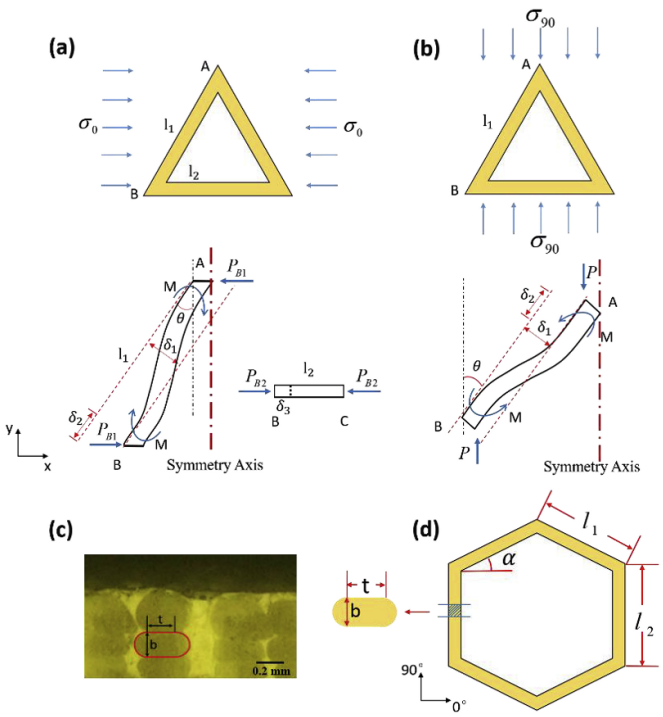

Figure 4. (a) Triangular element deformation under loading in the 0° direction. (b) loading in the 90° direction. (c) Optical image and geometry of the cross section of printed structure. (d) Hexagonal element of a two dimensional model of printed structure. Reprinted from [66], Copyright 2019, with permission from Elsevier.

Maxwell–Wiechert model to simulate its behavior. Results are compared with experiments, having a good agreement. Figure 4 shows the schematic representation of the model developed based on triangular elements.

Recently, Li *et al* [39] proposed a thermo-viscoelastic model to capture the initial dissociation of sub-entanglements, slipping, and orientation of polymer chains during the cyclic shape memory effect (CSME). For this purpose, the authors included a temperature-dependent stress threshold value and degree of orientation of the polymer chains in the constitutive model. According to the results, this model effectively describes the nonlinear stress–strain curve and the irrecoverable strain during CSME.

Although the last models accurately represent the deformation process of 4D printed polymer materials, they lack process parameters that influence the macroscopic behavior. Based on the multi-branch model in [67], Zhao *et al* [40] proposed a rheological model to predict the shape memory characteristics and corresponding degradation behaviors of stereolithography printed thermoresponsive structures. This model included process parameters, such as layer thickness and scan speed, showing a considerable impact on the shape memory performance of the printed parts. Furthermore, the results showed an outstanding accuracy prediction for the shape fixity and free recovery of 96.24% and 95.73%, respectively. The authors concluded that printing process parameters are crucial in defining shape memory performance, but the recovery temperature is a dominant factor influencing the shape recovery capabilities of 4D printed items [48, 49].

2.2. *Phenomenological models*

The continuum approach is the most effective and reliable method to describe macroscopic systems. This approach is a powerful tool for explaining several physical phenomena without detailed knowledge of their internal structure. For SMPs, a phenomenological model assumes that the body is composed of multiple continuum phases. After exposure to stimuli, these phases can transform into each other and thus exhibit corresponding properties. In contrast to rheological models, phenomenological models provide a clear physical interpretation.

However, expressing the viscosity and rate dependency effects on the SME within this system is challenging [68–71]. Most constitutive models for 3D printed polymers assume small deformations and use linear elasticity and yield criteria for orthotropic materials [72–76]. Among these studies, the one published by Zou *et al* [73] compared two modeling approaches: linear elasticity and transversely isotropic linear elasticity. However, these models do not predict the inelastic deformation process of 3D printed polymers under large deformation.

In addition, they did not include any links to the printing process. Therefore, though the process parameters have a significant influence on the macroscopic behavior of single-printed materials, modeling these parameters from a continuum perspective is a challenging task that has been solved by a few researchers.

Bodaghi *et al* [28] designed an adaptive metamaterial using functionally graded 4D printing. To describe the self-folding process, the authors reformulated the phenomenological model proposed in [77, 78] to study the fabrication parameters that affect the layer by layer programming process.

Although the authors identified five possible factors affecting the pre-strain values in the printed layers, they specifically evaluated the influence of printing speed and nozzle temperature on the layer by layer programming process and the resulting shape change. This model, coupled with a finite element formulation based on nonlinear Green–Lagrange kinematic relations, describes the material adjustment and deformation during the manufacturing stage.

Later, Hu *et al* [79] implemented a similar approach, in which they printed polymeric structures with self-bending features, eliminating the need for post programming. To achieve this, Hu and collaborators utilized a phenomenological model in [44, 77] and a Rietz based finite element formulation to address the thermomechanical properties of the SMP structures. In a further study, Bodaghi and Liao [80] adopted the model in [45] to simulate coupled hot and cold programming of polymers with reversible shape recovery features in the large strain regime.

Experiments showed elastoplastic and hyperelastic behaviors in the glassy and rubbery states. Moreover, the authors developed a computational tool by implementing a constitutive model and geometrically nonlinear finite element method. The governing equations are then solved using a return mapping procedure along with the risk and Newton–Raphson techniques.

Based on a study by Guo *et al* [81], Garzon–Hernandez [41] developed a hyperelastic constitutive model within a thermodynamically consistent framework for finite deformation, including the influence of anisotropic hyperelasticity related to a transversely isotropic distribution of porous, nonlinear response, and printing parameters. In this regard, void density explains the relationship between the layer height and mechanical response. The experimental results of the study showed that the stiffness and strength of printed SMPs depend not only on the void density but also on the number of layers. As a result, they proposed a softening model to replicate the relationship between the shear modulus and yield stress with the number of layers. The results indicated that the proposed model accurately represents the dependencies of the shear modulus and yield stress on the number of layers and raster orientation, as well as the overall mechanical behavior of 3D printed polymers.

Later, Li and Sun [82] proposed a model describing the rate of porosity change in porous materials, which improves the accuracy of the plastic stage prediction. They also introduced a function explaining how viscosity is affected by the loading rates and initial porosity (see table 2). Interestingly, the results matched the experimental data better than those for the study published by Garzon–Hernandez, confirming the effectiveness of Li's optimization and the porosity variation model.

Recently, Valizadeh and Weeger [84] proposed a concept called grayscale exposure (see figure 5), which accounts for the influence of the time and light intensity parameters on the final mechanical properties by changing the degree of monomer conversion. This new concept was introduced into a phenomenological visco-hyperelastic constitutive model for grayscale masked vat photopolymerization printed materials at finite deformations. Among the advantages of this formulation, the authors mentioned the reduction in parameter design and printing time owing to the correlation between exposure time and grayscale.

3. Multi-printed materials

Although some studies have demonstrated the use of single materials for 4D printed structures, the success of 4D printing resides in multiple materials [85]. Most researchers consider that using multiple materials in a single printed structure can provide superior features compared to single materials. These advantages include large actuation angles, better shape fixity, faster shape recovery, multifunctionality, and lightweight [31, 86]. Multi-printed materials are offshoots that combine a passive layer (e.g. paper) and an active layer (e.g. SMPs, Elastomers) to obtain self-sensing or self-actuating operations.

In particular, self-actuation can be achieved by arranging both layers to generate mismatch forces and guiding them in the desired direction. The strain mismatch between both layers is induced by the difference in some physical properties (e.g. Coefficient of Thermal Expansion (CTE) and swelling ratio), causing a phenomenon termed eigenstrain, in a way similar to how bimetals work. Therefore, multi-printed materials are the choice for 4D printing technology and represent the largest section of this review.

Understanding the deformation mechanisms of multi-printed materials to develop better functional structures remains an open challenge. Most of these mechanisms, such as folding, twisting, bending, corrugating, and stretching, have been analytically investigated by modifying the Timoshenko bimetal theory [87]. However, as 4D technology is 4D space-time dependent, this model does not capture the time-dependent behaviors of these materials (except in some exceptional cases). In addition, other approaches use the plates and beams theory without considering time dependence [88]. Herein, we follow a categorization similar to that proposed by Momeni and Ni [85]. This section classifies the models based on the approach used to describe the deformation mechanisms. These analytical approaches include pure geometry, the Euler-Bernoully beam theory, Timoshenko bimetal theory, and plate theory.

3.1. Geometrical models

Geometrical models are elementary and usually measure one of the crucial parameters related to the shape, such as the radio's curvature or the bending angle. Raviv *et al* [89] designed a complex self-transforming structure that changes over time in response to environmental interaction. For the folding behavior, the authors modeled each join using two disks and calculated the length between them according to their distance from the center of rotation.

Moreover, they further assumed that the center link remained fixed when the joint was deformed. This enables the

Table 2. Process parameters included in constitutive models.

Equation	References
$\zeta = \zeta_\infty[1-\exp(-\alpha/t)]$ $f = \frac{\sigma_{eqv}^2}{\sigma_0^2} + 2v_f q_1 \cosh\left(q_2 \frac{\sqrt{3}}{2}\frac{\sigma_{kk}}{\sigma_0}\right) - (1+(q_1 v_f)^2) = 0$ in [83] $\sigma_0 = (1-\zeta)(\sigma_y + (\sigma_s - \sigma_y)[1-\exp(-\mathbf{H}\epsilon_p)]$ ζ: softening variable ζ_∞: dimensionless maximum softening $\alpha = (Z-1)$ with Z being the number of layers t: softening saturation parameter q_1, q_2: material parameters that control the dependency with the porosity σ_{kk}: transverse hydrostatic stress to filament direction σ_y: yield stress σ_s: saturation stress $\mathbf{H}$: softening parameter ε_p: equivalent plastic strain	[41]
$\mathbf{l}_v = \frac{\nu}{\sqrt{2}\eta_0\nu_0(1-\xi_\eta)}\boldsymbol{\sigma}$ $\zeta = \zeta_\infty[1 - C_\eta \exp(-(Z-1)/t_\eta)]$ $C_\eta = A_1 \exp(-A_2\nu_{f0})$ ζ: softening variable ζ_∞: dimensionless maximum softening Z: number of layers t_η: softening saturation parameter A_1, A_2: constants C_η: influence of the filament thickness on the viscosity $\mathbf{l}_v$: viscosity velocity gradient component in the current configuration ν: loading rate ν_0: constant of the reference loading rate η_0: viscosity constant ν_{f0}: initial porosity	[82]
$\hat{H}_e = G^2 \cdot t$ $H_e = E_e^2 \cdot t$ $\hat{H}_e$: grayscale exposure H_e: radiant exposure E_e: light intensity G: grayscale value t: duration of the irradiation per layer	[84]

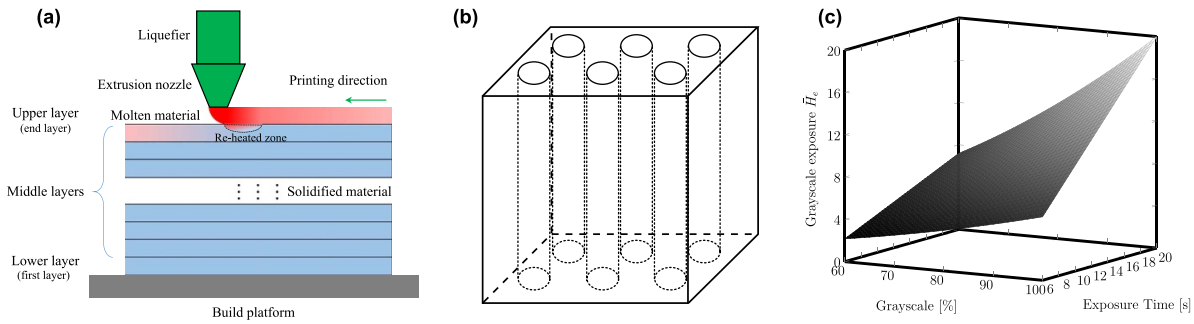

Figure 5. Schematic of process parameters included in constitutive models: (a) Layer thickness, nozzle temperature, nozzle speed. Adapted from [28], Copyright 2017, with permission from Elsevier. (b) Unidirectional aligned porous. Adapted from [41], Copyright 2020, with permission from Elsevier. (c) Schematic of grayscale exposure over grayscale and exposure time. Adapted from [84], Copyright 2022, with permission from Elsevier.

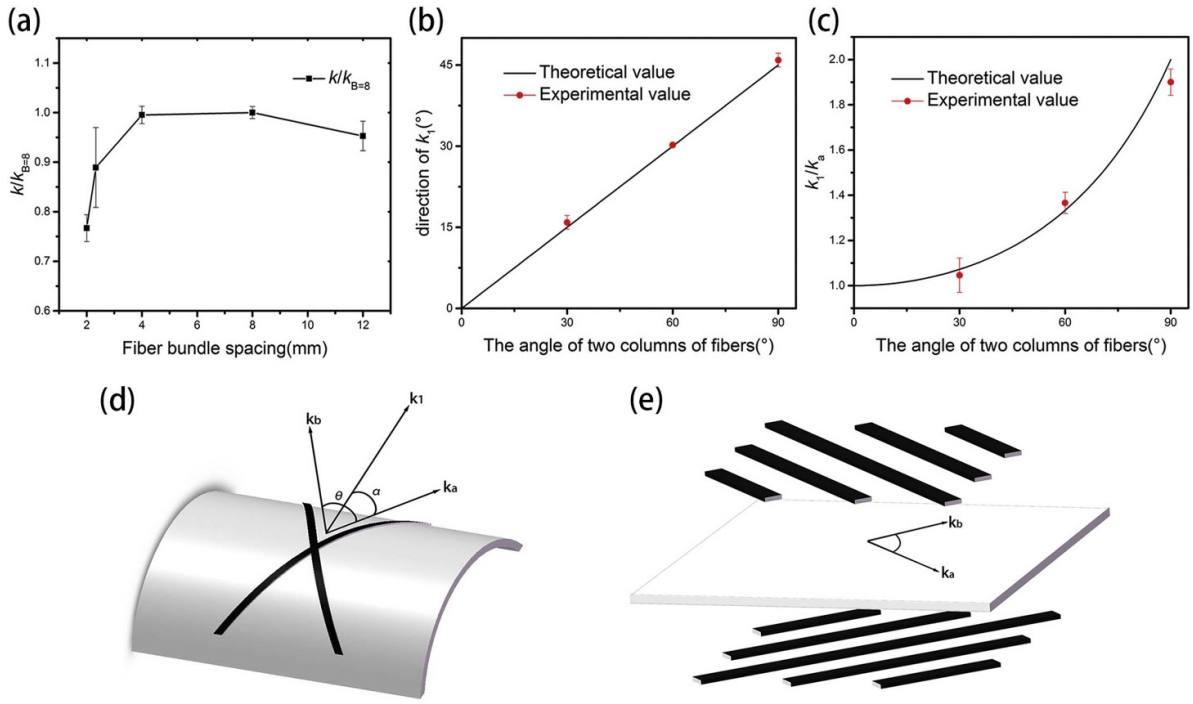

Figure 6. (a) Relationship between the curvature and the fiber bundle spacing, indicating that the curvature is in a stable state when the fiber bundle spacing is between 4 and 12 mm. (b) and (c) Relationship between the curvature direction and the angle of the fiber bundles. (d) and (e) Schematic diagrams of the last equations shown in table 3. Reprinted from [92], Copyright 2018, with permission from Elsevier.

estimation of the radius of the folding angle α and determines the total length l of the fixed structure as a function of the number of disks, diameter, and thickness of each disk. Once stretching is considered in the system, two angles on both sides of the bar, denoted as α and β are evaluated.

Deng and Chen [90] proposed a 2D origami self-folding structure using polystyrene film as an active layer and a photocurable resin on the top as a passive layer to control the folding behavior. In this study, the authors assumed that the energy generated in the contraction of the active layer leads to the deformation of the passive layer. Additionally, the passive layer blocks heat transfer from the environment to the bottom part of the polystyrene. Therefore, though the bottom constraining effect plays the principal role, the strain mismatch effect generated between both layers also contributes to the self-folding behavior. For the folding hinge analysis, the authors supposed that the lengths at the interface of the two layers are the same after the stimulus, allowing equal strains for both layers. For the energy conservation function, Deng and collaborators described the energy used in generating the deformation of the constraint layer from two approaches, elastic and plastic deformation.

Teoh *et al* [91] created flower petals using a mixture of VeroWhitePlus and TangoBlackPlus. Although fracture of the functional structure during shape-settings procedures is not abnormal, the authors developed a model to avoid this phenomenon. The model proposed depends on strain failure and thickness. As the strain failure can be measured with experiments and is constant, the thickness can be modified to avoid fracture. However, because of the radio domain, this model fails to describe the bending radius of materials with a strain greater than 100%.

Wang *et al* [92] proposed a bilayer composite material with embedded continuous fibers that can achieve programmable deformation with high accuracy. By carefully designing the fiber trajectories, the authors were able to control the deformation of deployable surfaces with minimal error between theoretical and experimental values. The size of the principal curve is determined by the angle between intersecting fibers, while the bisector of that angle determines the direction of the curve (see figure 6). By adapting the model based on the final shape, the authors were able to describe the bending behavior of the material.

Odent *et al* [93] fabricated hydrogel based actuators with anisotropy behavior to provide controllable motion. Anisotropy is generated by changing the surface area to volume ratio across the z-axis, allowing a higher swelling ratio at larger time scales. To describe the bending/unbending behavior, the authors used perhaps the simplest geometry relation, calculating the bending curvature from the radius r of the imaginary circle drawn around the actuated object.

Zeng *et al* [94] proposed a bilayer helical structure made of heterogeneous layers. Assuming no relative movement between both layers during deformation, the authors modeled the twisting behavior as a helix strip with a projection angle θ following a helical line. The spiral curvature k and shear stress τ of the structure can be referred to in table 3

Moosabeiki *et al* [95] proposed a design approach to harness anisotropic deformation of the printed filaments and micro defects generated during the printing processes to

Table 3. Representative geometrical models.

Equation	References
$\alpha \approx \frac{Nd}{r}, l \approx \alpha\left(r+\frac{D}{2}\right) \approx \alpha\left(\frac{Nd}{\alpha}+\frac{D}{2}\right) = Nd+\frac{\alpha D}{2}$ r: folding radius α: folding angle N: number of disk d: disk thickness D: disk diameter l: total length	[89]
$\alpha = K\sqrt{\frac{L^2 h}{d^3}}, K = \sqrt{\frac{24(1-\nu^2)\mu\rho q}{E^T}}$ α: bending angle K: coefficient related to the temperature and material properties h: thickness of the active layer d: thickness of the passive layer L: length of the bilayer ρ: density of the active layer q: unit releasing energy of the active layer μ: mass shrinking ratio of the active layer ν: Poisson ratio of the passive layer E^T: bending modulus of the passive layer cured under temperature T	[90]
$r = \frac{[(1/\epsilon_R)-1]t}{2}$ $\epsilon_R = \frac{L_R - L_0}{L_0}, L_R = R\cdot\theta$ r : bend radius ϵ_R: Strain at the surface t: thickness θ: bending angle L_R: original length L_0: bending length at the surface R: external radius	[91]
$\Delta e \approx \left(k_a - k_1\cos^2\alpha\right)^2 + \left(k_b - k_1\cos^2(\theta-\alpha)\right)^2$ $\alpha = \frac{\pi}{2}-\theta, k_1 = \frac{k_a}{\sin^2\theta}$ $\alpha = \frac{\pi}{2}, k_1 = \frac{k_b}{\sin^2\theta}$ Δe : strain energy density α : surface curvature direction k_1 : surface curvature magnitude θ: angle of two columns of fiber bundles k_a, k_b : surface curvatures	[92]

create curved geometries from 2D flat disks. To describe the out of plane deformation, the authors developed an empirical model to calculate the magnitude of the maximum deformation from the anisotropic expansion factor of the microstructures. Moreover, they explored its potential application in drug delivery systems.

3.2. Euler-Bernoulli beam theory

Another approach that scientists have used to describe the deformation mechanisms of multi-printed materials is the classical Euler–Bernoulli beam theory. Although this theory is mathematically simple, it does not consider the temporal dimension inherent in 4D printed polymer materials due to its multiple assumptions.

Ge *et al* [96] fabricated active composites with SMP fibers printed in an elastomeric matrix to use them as intelligent hinges enabling origami folding patterns. The bending behavior of the hinges resulted from the strain mismatch produced by both layers. Thus, the matrix layer was modeled as a simple elastomer, and the other layer was a unidirectional fiber-reinforced lamina.

Wu *et al* [97] proposed a bilayer composite fabricated of different SMP fibers embedded into an elastomer matrix. Owing to the difference in glass transition temperatures (T_g), the authors controlled the deformation order of the structure. Moreover, Wu and collaborators showed that guiding bending deformation is possible by adjusting the volume fraction of the fibers.

Wang *et al* [98] fabricated soft grafting mechanisms with different architectures made of a polymer-paper bilayer composite. The authors printed unidirectional polymer fibers on a paper substrate to trigger anisotropy and bending deformation in the transverse direction of the fibers. Furthermore, even though the polymer layer shrinks significantly, there are no wrinkles in either surface layer. This is because the polymer layer is printed layer by layer, allowing a progressive increase in the deformation contraction from the bottom to the top layer of the polymer. Nonetheless, Wang and collaborators consider the contracting deformation in the middle of the polymer layer as the contracting deformation of the entire layer, whose thickness is assumed to remain constant during the bending deformation to simplify the model.

3.3. Timoshenko bimetal theory

The Timoshenko bimetal theory is the most recurrent equation implemented by researchers to model the morphing behavior of 4D printed polymer materials. However, although this equation leads to a good approximation of the experimental observations, it fails to capture the time-dependent behavior inherent in these structures. Only accomplish this in very few exceptional cases or selected linear regions [85]. Furthermore, the Timoshenko bimetal model lacks generality for different materials and stimuli, making it not the best choice for model 4D printed bilayers.

Inspired by nature, Zhang *et al* [99] exploited the internal strain in printed polymers to fabricate functional structures composed of PLA strips printed on a paper substrate, mimicking the leaf vein structure. In addition to this proof of concept design, the authors proposed helical and corrugated structures using the same deformation mechanism principle. During the deformation process, the bilayer initially folded upward when exposed to high temperatures. However, as the temperature increases, the composite sheet bends in the opposite direction, making it almost flat after reaching equilibrium. The authors attributed this to the release of internal stress in the 3D printed material, which counteracts the deformation caused by the mismatching CTE of the composite materials.

To demonstrate the practicability of 4D printing, Su *et al* [100] proposed a pattern bilayer printed on a commercial polymer, SU-8, on an aluminum substrate. To fabricate an active region on the pattern, a gradient of cyclopentanone concentration was created in the bilayer as the swellable medium. Although the Timoshenko formula uses coefficients of thermal expansion that are deficient in replicating the SU-8 morphing behaviors, the bending mechanism disclosed by the Timoshenko theory presented in Su's work is similar to that reported in a prior study [101].

Experiments have shown that the coefficients of thermal expansion do not influence the bending curvature although they have a bearing in the bend direction. Instead, it is apparent from Timishenko's theory that the thickness governs the model deformation. In addition to the thickness, the lengths also play a paramount role in the underlying morphing behavior. Therefore, the authors fabricated strips with various longitudes ranging from 4 to 12 mm to verify a possible relationship. They found no correlation between strip length and curvature, although the curvature angle was affected by different longitudes.

Inspired by botanical systems, Sydney Gladman *et al* [88] printed composite hydrogel architectures with localized anisotropy caused by the alignment of cellulose fibers in the printing patterns. The authors presented an extension model from the plate and shell theory to characterize curvature behavior, which combines aspects of the classical Timoshenko model with a tailored metric-driven method [102, 103] that employs anisotropic swelling to regulate the embedding of a complex surface.

Owing to the superb alternative, spontaneous deformation of polymers offers compared to traditional approaches for 3D biofabrication. Stroganov *et al* [104] fabricated a 3D cellular film composed of three layers; N-isopropyl acrylamide at the bottom, stearyl methacrylate and benzophenone acrylate (PSMA) in the middle, and a thin-patterned layer of polyethyleneglycol (PEG) at the top. This film provides a combination of homogeneous distribution of cells and microporosity [105] owing to the fabrication process. To describe the folding behavior, the authors assumed an elastic stress proportional to the thickness of the hydrogel and replaced the CTE with the swelling degrees of both polymers.

Combining an elastomer on the top of a SMP, Yuan *et al* [106] fabricated a laminate capable of evolving into a 3D structure due to the mismatch strain between both layers. In this study, the multibranch model was used to represent the thermomechanical properties of the SMP, with one equilibrium branch and numerous thermoviscoelastic nonequilibrium branches organized in parallel [107, 108]. Meanwhile, the elastomer material is described using a linear elastic model. To further simplify the model and predict the bending curvature, Yuan and collaborators modified the Timoshenko bimetal theory to include the thermal strain difference between the elastomer and SMP at high temperatures. The authors discovered that the locking effect weakens with a broader glass transition area during cooling because the rate of modulus increase with temperature becomes sluggish and is not sufficient to lock the form. Consequently, if one wants to hold the deformed shape, a sharp glass transition is preferred. Finally, the authors argued that a substantial thermal strain difference, lower overall thickness, and optimal thickness ratio will all favor a higher bending curvature.

Based on the plant leaf architecture, Momeni *et al* [109] designed a multifunctional turbine blade capable of reversible bend-twist coupling (BTC). The proposed design concept aims to reduce the inherent flutter instability challenge by achieving flexibility only during the shape shifting process. This allows

for a more stable structure because the initial and final shapes can be as rigid as needed.

Moreover, to establish the relationship between the printing paths and the desired BTC shape, the authors modified the Timoshenko bimetal model to describe the BTC behavior, including a rheological element to describe the equivalent linear CTE derived from the classical Kelvin-Voigt model [99, 110]. After the shape-morphing process, the deformed blade is a function of the global bending angle α and the twist angle β. Finally, α and β describe the blade's overall bending-twisting behavior by adding the lateral and principal contributions from the leaf architecture.

The design and fabrication of shape-morphing structures remain an issue because of the complexity of controlling the metric tensor in space and time. That is, it is possible to program arbitrary shapes in three dimensions, defining how the lengths and angles change everywhere. Therefore, Boley *et al* [111] proposed a heterogeneous open-cell lattice composed of bilayer ribs to achieve independent control of the parameters. Introducing four different materials within the cross-section of each rib allowed control of expansion across the thickness and width, and hence, control of intrinsic and extrinsic curvatures. The curvature response of these bilayers to thermal changes resides in a modified Timoshenko model, capturing a space of dimensionless curvature increments. This study achieved a lattice with a significant amount of local linear growth, which could be varied independently across the lattice and in each of the two orthogonal lattice directions. Furthermore, the out of plane bending control minimizes elastic frustration, simplifies the inverse design, and broadens the range of shapes achievable over previous works [88, 112].

Inspired by biological systems, Ji *et al* [113] later developed hydrogel based architectures with complex and controllable shape deformations by introducing secondary grooves on one side of the feature structures. This leads to bending or twisting deformations owing to the local curvatures caused by asymmetric swelling. The authors used the classic Timoshenko theory to predict the self-folding behavior with no further modifications.

Reversibility (two-way) allows 4D printed polymer materials to eliminate the need for physical interference, as the programming process is driven by external stimuli, which permits the structures to be actuated in multiple cycles. As one of the main drawbacks of 4D printing technology [114], this capability has been frequently exploited with hydrogels, although not often with shape memory composites.

To overcome this, Lee *et al* [115] proposed a reversible 4D printing actuation method. In this method, during the programming step, two stimuli (ethanol and heat) were employed to trigger a shapeshift from permanent form one to permanent shape two. Moreover, the elastomer layer performs two functions: it swells and causes internal stress during the programming stage, while it converts the stored potential energy into elastic energy, pulling the bilayer back to its original shape during the recovery process. For the curvature of the bilayer strip, the authors developed an equation based on the Flory–Rehner, Peppas, and Timoshenko models. Among the assumptions made, they found that differences in strain due to the contrast in thermal expansion coefficient are neglected [116], and the cross-section normal to the longitudinal axis remains plane during bending.

Recently, Feng *et al* [117, 118] presented a method for controlling a self-helix structure composed of a strip bilayer with rectilinear and wiggle patterns. In these studies, the authors described the deformation process of a PLA bilayer using the phase transition model described by Lu *et al* [119]. During deformation recovery, the release of stored strain energy results in internal stress, which leads to shape memory deformation [49]. Although Timoshenko's theory is used to describe the curvature of a helical actuator, if both thicknesses are equal, this equation can be further simplified [120], as shown in table 4. Moreover, Feng and collaborators argued that the printing temperature had the greatest influence on the curvature, whereas the printing layer height had the greatest impact on the gradient angle.

3.4. Plate theory

Finally, the Classical Laminate Theory, in combination with Kirchoff's plate theory, is another approach frequently used to describe the shape-shifting behavior of multi-printed material structures [123]. Although this approach has become the cornerstone of all subsequent studies, its multiple assumptions cause it to lack accuracy. Among its premises, it ignores interlaminar stresses and strains, which play a vital role in the balance of the overall stress field. Moreover, these simplifications create an inconsistency in which the stresses appear imbalanced at the edges of the laminate and the through the thickness deformation is ignored.

To overcome these limitations, Deshpande *et al* [124] presented a new analytical formulation that adopts the Reissner–Mindlin theory. In addition to the transverse deflection, this theory includes two other independent factors: rotation about the y-axis θ_x and rotation about the x-axis θ_y, allowing the in-plane stress τ_x at the edges to be balanced by interlaminar stresses. This leads to a better approximation of the laminate deformation and makes it capable of explaining the free edge delamination failure.

Song *et al* [125] proposed a reduced plate theory model to capture complicated deformations, adding the influence of the printing process. The authors developed a stable convergent, and efficient method capable of forecasting deformation patterns such as twists and helices. To simplify the bending model problem, the Kirchhoff assumption was applied; therefore, a modified Timoshenko bimetal model was used to describe the deformation mechanism. By considering the thermal expansion anisotropy, Song and collaborators employed an energy density function method to describe the complex deformation based on previous studies [126, 127]. Similar approaches have been applied to the energy methods, as shown in table 5.

Sydney Gladman *et al* [88] were inspired by botanical systems and created a biomimetic hydrogel composite encoded with localized swelling anisotropy. This composite could generate complex shape changes when immersed in water. Therefore, the authors extended the classical Timoshenko bimetal model to 2D by introducing an angle h between the

Table 4. Representative Euler–Bernoulli and Timoshenko models.

Equation	References
$\epsilon(z) = \epsilon^0 + kz, M = \int \sigma z \mathrm{d}A = \int zE(\epsilon^0 + kz)\mathrm{d}A$ $= E\epsilon^0 \int z\mathrm{d}A + kE \int z^2 \mathrm{d}A \Rightarrow M = kEI = \frac{EI}{r} = \frac{\theta EI}{l} \Longleftrightarrow \theta = \frac{ML}{EI}$ ϵ: strain ϵ^0: strain at the mid-axis σ: stress z: distance from the neutral axis A: cross-sectional area of the beam k: curvature θ: bending angle r: curvature radius E: Young's modulus I: Second moment of inertia M: moment L: length	[96–98]
$\frac{1}{\rho} = \frac{6(\epsilon_2 - \epsilon_1)(1+m^2)}{h[3\times(1+m^2)+(1+mn)(m^2+\frac{1}{mn})]}$ ρ: radius of the curvature ϵ_1, ϵ_2: thermal expansion coefficient of the two layers m: ratio of the thicknesses of the two layers n: ratio of the Young's of the two layers h: thickness of the bilayer	[92, 100, 104, 106, 111, 113, 121, 122]
$\theta_i(l_i, t') = -6\alpha_{\mathrm{eff}} T t'(1-k') \frac{l_i}{h_{m,i}} \frac{E'_{pm} h_{pm,i} b_{pm,i}(h_{pm,i}+1)}{(E'_{pm} h_{pm,i}+1)(E_{pm} b_{pm,i} h^3_{pm,i}+1)}$ $\beta = \theta_0(l_0, t') + \cos(\gamma) \times (\theta_1(l_1, t') + \theta_2(l_2, t') + \theta_N(l_N, t'))$ θ: bending angle β: blade bend angle γ: angle between the main vein and lateral veins $h_{pm} = h_p/h_m$: thicknesses ratio of the two layers $b_{pm} = b_p/b_m$: widths ratio of the tow layers. $E'_{pm} = E_{pe}/E_m$: Elastic modulus ratio of the two layers (E_{pe} is the elastic modulus of the active layer above its glass transition temperature) l: length of the composite strip t': time starting from the point of the glass transition temperature T: Heating rate p: printed polymer m: membrane of paper	[109]

two layers and Gaussian curvatures. The classical Timoshenko bimetal model can be obtained when h approaches 0°.

3.5. Modeling the time dependence behavior in bilayer structures

The fourth dimension (time) is the most important feature of 4D printed polymer materials. Therefore, its incorporation in the constitutive models is essential to forecast the shape change behavior of bilayer structures in a time interval. Successful models capable of predicting deformation before the fabrication process can improve the workflow and eliminate the trial and error method often employed to identify the structure needed for the final shape [132].

Although the 4D printing concept arose in 2013 in a TED talk by Prof. Tibbits [133], it was not until 2020 that the time-dependence behavior was incorporated for the first time in a bilayer model [85]. In the last section, most of the models rely on Timoshenko's theory to describe their deformation mechanisms, though it does not consider time as a variable. Moreover, the available models lack generality and are customized according to the final structure's application. Therefore, Momeni and Ni [85] proposed the three laws of 4D printing and developed a bi-exponential model to capture this additional dimension. According to the authors there are three general laws that govern the shape-morphing behaviors of almost all 4D multi-printed materials. In this article, we summarized the three laws as follows:

Table 5. Representative plate theory models.

Equation	References
$(D^2\mathbf{y}, D^2\mathbf{w}) + \sum_{i,j=1}^{2} (\partial_i \partial_j \mathbf{w} \cdot (\partial_1 \mathbf{y} \times \partial_2 \mathbf{y}), Z_{ij}) = 0$ $D^2\mathbf{y}$: Hessian of $\mathbf{y}$ $\mathbf{y}$: deformation of the mid-surface of the bilayer structure at equilibrium $\mathbf{w}$: transverse deflection Z_{ij}: metric tensor	[125, 128]
$H = c_1 \frac{\alpha_\parallel - \alpha_\perp}{h} \frac{\sin^2(\theta)}{c_2 - c_3 \cos(2\theta) + m^4 \cos(4\theta)}$ $K = -c_4 \frac{(\alpha_\parallel - \alpha_\perp)^2}{h^2} \frac{\sin^2(\theta)}{c_5 - c_6 \cos(2\theta) + m^4 \cos(4\theta)}$ H: mean curvature; $H = \frac{1}{2}\text{trace}(k)$ k: curvature tensor in [88] K: Gaussian curvature; $K = \det(k)$ $\alpha_\parallel, \alpha_\perp$: longitudinal and transverse swelling strains θ: angle between the two layers in the bilayer h: sum of the layer thicknesses m: ratio of the layer thicknesses c_i: function of m and the elastic moduli	[88]
$\Pi = \int_{-L_x/2}^{L_x/2} \int_{-L_y/2}^{L_y/2} \frac{1}{2} \begin{bmatrix} \epsilon_0 & k \end{bmatrix} \begin{bmatrix} A & B \\ C & D \end{bmatrix} - \begin{bmatrix} \epsilon_0 & k \end{bmatrix} \begin{bmatrix} M_t \\ N_t \end{bmatrix} \text{d}y\text{d}x$ $\epsilon_0 = \begin{bmatrix} \epsilon_{x0} \\ \epsilon_{y0} \\ \gamma_{yz0} \\ \gamma_{xz0} \\ \gamma_{xy0} \end{bmatrix}, k = \begin{bmatrix} -\partial\theta_x/\partial_x \\ -\partial\theta_y/\partial_y \\ 0 \\ 0 \\ -(\partial\theta_x/\partial_y + \partial\theta_y/\partial_x) \end{bmatrix}$ ε_0: mid-plane strains k: curvature tensor M_t, N_t: moment and normal force vectors	[124, 129]
$\vec{\alpha}_k \Delta_T = -\frac{2}{3} \frac{(h_k^3 - h_{k-1}^3)}{(h_k^2 - h_{k-1}^2)} \vec{k}$ $\vec{\alpha}_k \Delta_T$: thermal strain k: curvature vector h_k: height coordinates of the respective kth layers	[130, 131]

(i) Exist an expansion between the active and passive layers.
(ii) There are four types of physics: mass diffusion, thermal expansion, molecular transformation, and organic grown.
(iii) The time-dependent behavior is governed by two constants: H_{II} and τ_{II}. The first one depends on the viscosity induced at the interface and Young's moduli of the active and passive layers. The second is introduced for the strain resulting from the mismatch-driven stress.

In the second law, Momeni and Ni [85] derived the following equation based on the four types of physics (see equation (1))

$$\begin{cases} \epsilon_{\text{mass-diffusion}}(t) = C_1 [1 - \exp(-t/\tau_1)] \\ \epsilon_{\text{thermal-expansion/contraction}}(t) = C_2 [1 - \exp(-t/\tau_2)] \\ \epsilon_{\text{molecular-transformation}}(t) = C_3 [1 - \exp(-t/\tau_3)] \\ \epsilon_{\text{organic-grown}}(t) = C_4 [1 - \exp(-t/\tau_4)] \end{cases} \Longrightarrow C_j [1 - \exp(-t/\tau_j)] \quad (1)$$

where C_j and τ_j $(j = 1,2,3,4)$ are constants that depends on factors described in [85]. Finally, the time-dependent behavior (in terms of curvature) is obtained by equation (2) where $k(t)$ is the curvature induced under stimulus; r is the radius of curvature; h, a_1, and a_2 are thicknesses; E_1 and E_2 are Young's modulus, and I_1 and I_2 are the second moments of area. H_I is a constant that depends on Young's modulus of the active and passive layers and the amount of mismatch driven stress generated at the interface. τ_I is a time constant that depends on the viscosity induced at the interface and Young's modulus. H_{II} and τ_{II} are respectively equivalent to C_j and τ_j (j = 1, 2, 3, 4) shown previously. To derive this equation, Momeni and collaborators considered Timishenko's bimetal model and its basic assumptions. For compatibility, the length of both layers at the interface is assumed to be the same after stimuli. Therefore, their strains must be equal. Furthermore, to model the friction generated at the interface, the well-known momentum equation is expanded for each layer [85]

$$k(t) = \frac{1}{r}(t) = \frac{H_I\left(1-\mathrm{e}^{-t/\tau_I}\right)+H_{II}\left(1-\mathrm{e}^{-t/\tau_{II}}\right)}{\frac{h}{2}+\frac{2(E_1I_1+E_2I_2)}{h}\left(\frac{1}{E_1a_1}+\frac{1}{E_2a_2}\right)}. \quad (2)$$

Later, the authors compared their proposed model with the Timoshenko and a mono-exponential model for multiple stimuli such as heat, moisture, solvent, photochemical, photothermal, and ultrasound. Results showed a good agreement with the experimental data. According to the remarks, when both time constants are large, the proposed model tends to be linear, and, in this case, both the presented model and Timoshenko bimetal model work. Additionally, both equations provide similar analyses for time-independent behaviors, such as the effect of thickness on curvature. In general, Momeni's study proposed a new way to describe the time-dependent behavior of unidirectional curvature, which is a fundamental building block of shape-shifting in multi-printed materials structures.

4. The role of ML inferring constitutive relations

AM, typically known as 3D printing, is a promising digital approach for industrial production that enables the creation of lighter, stiffer parts and systems. By fabricating objects layer by layer from digital designs, AM offers several advantages in contrast to subtractive manufacturing methodologies. These advantages include the construction of complicated geometries, the generation of unique material characteristics (e.g. dislocations), material waste reduction, and fabrication costs [134]. However, even with its broad adoption in the industry, unique defects like porosity, microstructural anisotropy, distortion, and inconsistency in product quality limit their use in other sectors [134–136].

Given their complexity, it is impractical to effectively predict the entire AM process with only analytical methods [137–140]. Therefore, the integration of ML into AM represents a significant advancement in optimizing and improving the capabilities of this technology. Data-driven models have been used in AM due to their outstanding performance in data tasks such as classification, regression, and clustering (see figure 7). Whether designing high performance metamaterials, optimizing process parameters, monitoring in-process defects, or assessing quality and controlling products, ML models are present during the all-AM process [135, 141, 142].

Its main advantage over analytical methods is that ML models automatically learn the relationships between the input feature and output target based on previous data instead of constructing a long list of physic-based equations [143]. For this purpose, the artificial neural network (ANN) algorithm is the most widely used, though there are several ML model techniques available (see table 6).

As a result of the widespread use of digital data, increasing computing power, and improved algorithms, ML models are becoming more prevalent in diverse engineering fields. Although many ANN models have been used in the constitutive modeling of composite materials [145], there is still a gap in the literature regarding their use in SMPs and their composites.

Most studies on ML for SMPs have focused on ANN models to design new SMPs based on the desired recovery stress and glass transition temperature [146, 147]. For example, Yan *et al* [146] discovered a new thermoset SMP with high recovery stress and modest glass transition temperature using ML algorithms with a small dataset. ANN have also been used to predict dimensional errors during the 3D fabrication of SMPs [148, 149] and glass transition temperatures [150].

Owing to the reliance on 4D printing with smart materials, the lack of literature on ANN models in the constitutive modeling of SMPs has also delayed their integration into 4D printing to predict hierarchical relationships and crucial printing process parameters. Most studies applied ML methods to design 4D printed structures [151, 152]. For example, Su *et al* [153] provided a data-driven approach to accurately predict the final shape of structures based on geometrical features, such as curvature and curvature angle.

Predicting the thermomechanical properties of SMPs is paramount for validating new SMPs, and is essential for designing devices made of these materials. Despite extensive research dedicated to developing mathematical models, this task is often time consuming, and these models usually consist of many parameters that need to be determined through curve fitting.

To address this limitation, Wang *et al* [154] proposed a method for estimating these parameters using an ML algorithm based on single-value decomposition and an adaptive ANN. This method not only maintains the physical meaning of the constitutive models but can also be adapted to various models by adjusting the size of the neural network and the training set. Jordan *et al* [155] applied a hybrid modeling approach that integrates mechanism based and data based modeling techniques. To accomplish this, the authors utilized a backpropagation algorithm with Bayesian regularization to identify an optimized neural network function based on experimental data. Subsequently, the authors implemented a neural network in series with a temperature-dependent spring to describe the stress–strain response.

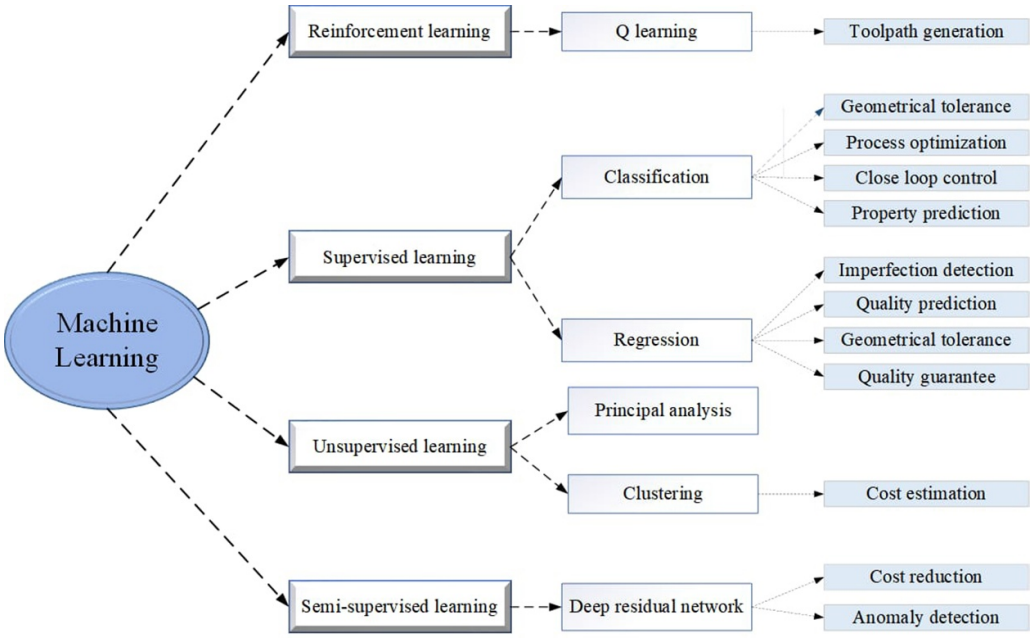

Figure 7. Diagram representation of ML applications on additive manufacturing.

Table 6. Different classifications of ML techniques. [144] John Wiley & Sons. © 2024 The Authors. Advanced Materials published by Wiley-VCH GmbH.

Category	Techniques
Supervised learning	Linear regression
	Logistic regression
	Support vector machine
	Decision trees (e.g. classification and regression tree)
	Random forest
	Gradient boosted trees (e.g. XG Boost, LightG BM, CatBoost)
	Neural networks (e.g. DNN, RNN, U-Net, RandLA-Net, LSTM)
	K.nearest neighbours (K-NN)
	Gaussian process modelling
	Ensemble learning (e.g. Adaboost, Bayes optimal classifier, bagging, stacking)
Unsupervised learning	K-means clustering
	Hier archical clustering
	Principal component analysis (PCA)
	Independent component analysis (ICA)
	Autoencoders (e.g, variational autoencoder)
	Gaussian mixture models
Semi-supervised learning	Self-training
	Multi-view training
	Generative adversarial networks (GANs)
	Domain advers arial neural network
Reinforcement learning	Q-learning
	Deep Q networks (DQN)
	Monte Carlo methods
	Policy gradient methods
	Actor-Critic

Recently, Ibarra *et al* [156] introduced an ANN model to predict the response of a polymer to thermomechanical cycles, varying temperatures, and applied stress over time. In this study, the authors compared different ANN models to determine which corroborated the experimental results with the highest accuracy. The results revealed that fully connected neural networks (FCNN) and convolutional neural networks (CNN) provided the most accurate predictions (see figure 8). However, they recommended using an FCNN owing to its low training time.

Efforts to describe the nonlinear nature of viscoelasticity problems using ML algorithms have gained attention over the

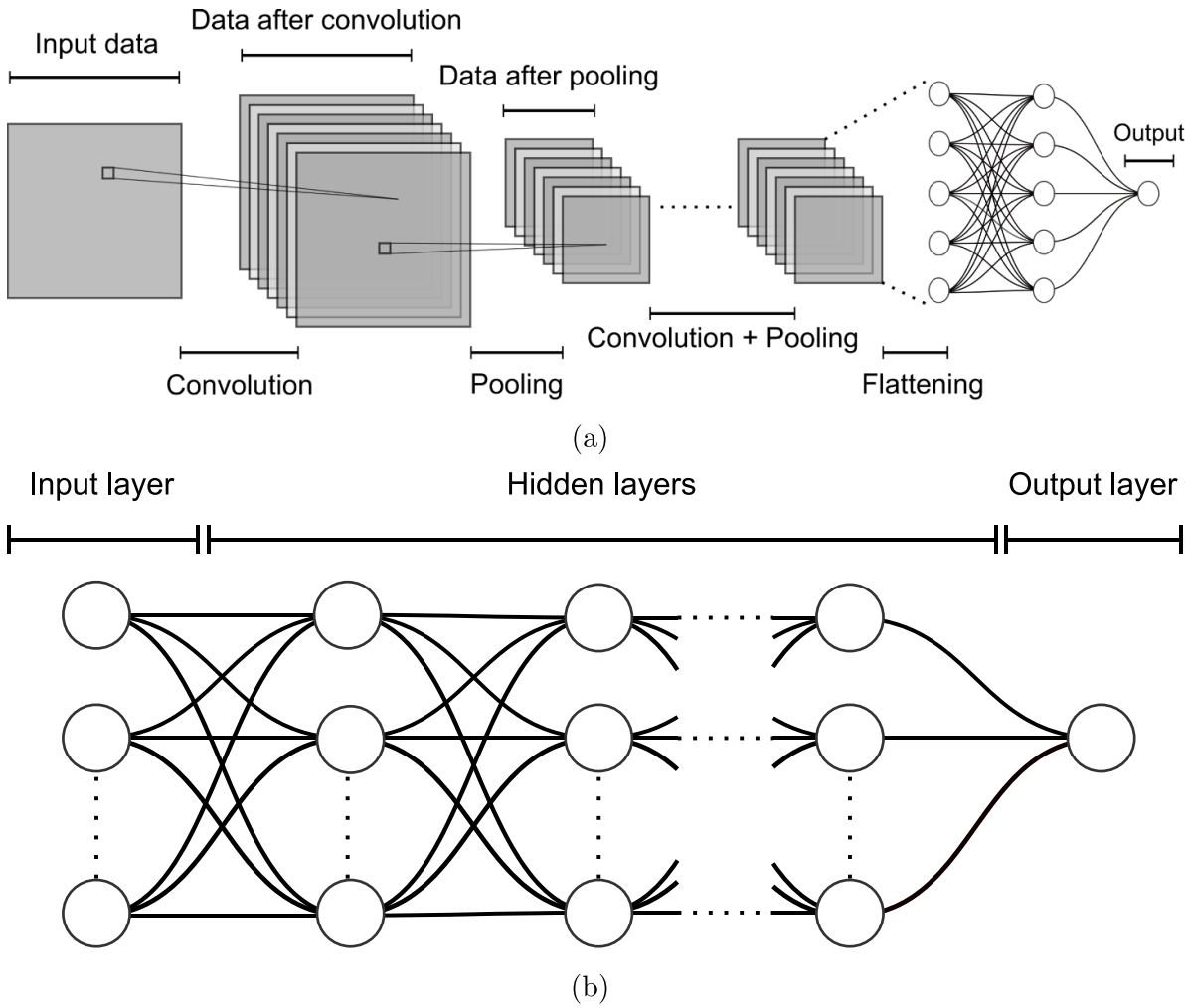

Figure 8. Visual representation of: (a) general convolution neural network (CNN) and (b) fully connected neural network (FCNN).

past few years. Traditional analytical approaches are cumbersome to solve and computationally expensive, and most are only available for one dimensional problems. Consequently, they have had a minor impact on the finite element analysis [157, 158].

As indicated by Jordan *et al* [155], these models share a common feature: the strain rate and temperature-dependent large-strain response are described through parametric functions. To be more precise, particular parametric forms are proposed for the functions that govern the quantitative model response based on either phenomenological considerations or physical assumptions. Data-driven modeling techniques such as ML avoid these issues by offering a flexible computational framework that infers constitutive relations from data rather than stating them in advance [159–161].

Moreover, modeling the time-history effects of viscoelasticity requires a neural network for temporal signal processing. Thus, recurrent neural networks (RNNs) and similar architectures have been used extensively. For instance, Oeser and Freitag [162] used an Elman network to model materials with time-history effects based on fractional differential equations under cyclic loading conditions. In this study, the authors reduced the computational effort by implementing RNNs with partially recurrent structures. As a result, signal flow in the network occurs forward, and memory fading is achieved through its internal feedback connection.

Instead of a constitutive model, Freitag *et al* [163] implemented RNNs with fuzzy data to explain the time-dependent material behavior using the finite element method. A similar approach was adopted in [164] to describe the inelastic behavior of rubber-like materials.

Based on [165], Abdolazizi *et al* [166] proposed a viscoelastic constitutive artificial neural networks (vCANNs) for anisotropic nonlinear viscoelasticity in the large-strain regime. By incorporating nonlinear strain coefficients and relaxation times as neural networks within the framework of the generalized Maxwell model, the vCANNs can adapt automatically during training.

The authors claimed that the accuracy of this physics-informed ML framework surpasses that of similar traditional approaches proposed in the literature [167]. Interestingly, they highlighted that this framework can describe strain-dependent relaxation curves accurately, which is often believed to be impossible for frameworks based on generalized Maxwell models with strain-dependent material parameters.

As ML methods continue to improve, 4D printing will benefit from better shape-changing predictions, more robust algorithms to infer constitutive parameters and a deeper understanding of multiscale relations.

5. Challenges and opportunities

Modeling the constitutive behavior of 4D printed materials is a fast-growing research field. Although 4D printing continues to rely on traditional analytical methods, the rapid pace at which data-driven techniques improve the inference of constitutive relations deserves attention. However, as with any other data analysis, these techniques are not exempt from unconscious biases, issues around reproducibility, or lack of objectivity [168]. As reviewed in this manuscript, many groundbreaking studies have been published in the last few years. For example, incorporate the process parameters in single-printed material models and use time as a variable in the bilayer materials. However, despite these modeling advancements, several challenges remain. In our opinion, these challenges include:

- *Damage evolution*: For fused deposition fabricated polymers, bonding between layers is not often perfect [169]. Therefore, these structures are prone to delamination after several shape-shifting cycles. For bilayers, this problem is even more common, diminishing the structural capacity to carry out heavier loads. Thus, developing models to assess damage evolution will allow the shape-shifting process to be repeatable and more feasible in the long term.
- *Data acquisition and accessibility*: Collecting reliable data is crucial for learning and validating constitutive relations in data-driven models, which can be challenging for 4D printed polymer materials under different conditions. Therefore, database solutions and relevant websites may allow a broad audience access.
- *Validation*: The validation of data-driven constitutive models and their ability to predict material behavior under different conditions is challenging and time consuming. The non-interpretable nature of these models can pose a challenge for engineers and scientists who want to analyze and comprehend their behavior.
- *Embedded anisotropy*: It is well-known that the FDM process embedded anisotropy into the final part by changing the printing direction. In the case of a multilayer material with different materials in different directions, the curvature would differ in each direction. Therefore, models integrating this anisotropy are crucial to accurately predict the deformation process and thus design better devices.
- *Generalization*: Constitutive models should be capable of generalizing to different materials, printing techniques, printing parameters, stimuli, and environmental conditions. However, gaining this level of versatility in analytical and data-driven models is a significant challenge that must be solved.
- *Topology optimization*: Most topology optimization methods focus on material reduction and improvement of mechanical qualities, leading to a reduction in cost. However, this might produce thermal expansion and contraction issues during and after printing.

Additionally, based on the content of this article, the following opportunities to improve these models are suggested:

- *Modeling in further dimensions*: Most of the models presented in section 3 reside in one dimension. Therefore, new approaches should extend these models to other dimensions. This offers the opportunity to gain a deeper understanding of how bilayers behave at different scales, thereby improving the accuracy of the models.
- *4D printing software*: Owing to the diverse range of 4D printing procedures, a new 4D printing software is essential. The development of software within the industry must consider fundamental factors such as smart material properties, printing techniques, deformation behaviors, geometry optimization, and architectural requirements of the products, as well as the shape-changing mechanisms inherent to 4D printing techniques.
- *Real-time control*: Using data-driven models within real time control systems allows adaptive structures that dynamically adjust their shapes along with changing operating conditions. This is particularly useful for applications in robotics, aeronautics, and defense.
- *Integration with AM*: Improvement over time will allow 4D printing technologies to consistently incorporate data-driven models into the AM process with real time optimizations.

6. Summary and future perspectives

In this study, we reviewed the critical role of constitutive theories in understanding and predicting the behavior of 4D printed polymer materials. These models, ranging from classical rheological to phenomenological and ML based approaches, provide a theoretical foundation for analyzing printed polymer materials' deformation and shape-shifting capabilities. Particular attention is given to those analytical solutions that consider printing process parameters in their models since this particularity improves our understanding of this disruptive technology.

Rheological models have been effective for a deeper understanding of shape memory performance and accurate predictions. These models, including process parameters such as layer thickness and scan speed, have considerably impacted the shape memory performance of printed parts. For instance, the work done by Zhao *et al* [63] based on the multibranch model is a notable example where rheological models provided outstanding accuracy in predicting shape fixity and free recovery rates. In another example, temperature-dependent stress thresholds and the degree of orientation of polymer chains have allowed for a better description of the nonlinear stress–strain curve and the irrecoverable strain during the CSME.

On the other hand, phenomenological models serve as a robust framework for capturing the macroscopic behavior of SMPs under several stimuli. These models, incorporating factors like printing speed, nozzle temperature, void density,

and porosity rate, have successfully simulated material adjustment and deformation during the fabrication.

Furthermore, ML techniques in AM, especially in constitutive modeling and parameter inference, present a novel approach to overcoming the complexities associated with traditional modeling methods. ML algorithms offer a promising route for improving the efficiency of 4D printing processes, accelerating the development of adaptive materials.

As discussed throughout this literature review, the constitutive modeling of 4D printed polymer materials is still in an early stage. Even though researchers have started adding printing parameters into their models or extending classical models, their inclusion and refinement is a challenging task that require further research and innovation. Therefore, we expect to see the following research in the upcoming years:

- Even with the relative success of rheological models, the recovery temperature remains a dominant factor influencing the shape recovery capabilities of 4D printed items, and the models still need to be expanded to represent the complex deformation processes of SMPs fully. Integrating these models with experimental data and considering additional process parameters will be crucial for further enhancing the predictability and reliability of 4D printed structures.
- While phenomenological models offer a powerful tool for explaining physical phenomena, the complexity of accurately representing the viscoelastic behavior of SMPs remains a significant challenge. Therefore, it is expected further refinement to accurately capture the viscoelastic and rate-dependent phenomena critical for these materials.
- An improved understanding of magneto-mechanical coupling requires studying particle interactions and interfacial effects on fillers to aid in material design [170]. For this, multiscale approaches can bridge the gap at the microscale to the macro-scale behavior of magnetic materials.
- Expanding the application of ML in AM to include not only constitutive modeling but also process optimization and quality control could significantly improve the precision, efficiency, and reliability of 4D printing.

Data availability statement

All data that support the findings of this study are included within the article (and any supplementary files).

Acknowledgments

This work is supported by the National Natural Science Foundation of China (Grant Nos.: 12372071, 12372070 and 12202181), the Aeronautical Science Fund (Grant No.: 2022Z055052001), the Natural Science Foundation of Jiangsu Province of China (Grant No.: BK20220325), the Fund of Prospective Layout of Scientific Research for Nanjing University of Aeronautics and Astronautics, and the China Scholarship Council (CSC) (Scholarship No.: 2021GXZ008546).

Conflict of interest

The authors declare no competing interests.

ORCID iDs

Jesus A Rodriguez-Morales https://orcid.org/0000-0002-9280-8562
Jianping Gu https://orcid.org/0000-0002-9069-2842
Hao Zeng https://orcid.org/0000-0002-1862-7878

References

[1] Wu P, Wang J and Wang X 2016 *Autom. Constr.* **68** 21–31
[2] Savini A and Savini G. G 2015 *ICOHTEC/IEEE International History of High-Technologies and their Socio-Cultural Contexts Conf. (HISTELCON) (Tel-Aviv, Israel, 18–19 August)* pp 1–8
[3] Lin D, Nian Q, Deng B, Jin S, Hu Y, Wang W and Cheng G J 2014 *ACS Nano* **8** 9710–5
[4] Ho C M B, Ng S H and Yoon Y-J 2015 *Int. J. Precis. Eng. Manuf.* **16** 1035–46
[5] Tay Y W D, Panda B, Paul S C, Noor Mohamed N A, Tan M J and Leong K F 2017 *Virtual Phys. Prototyp.* **12** 261–76
[6] Martin R L, Bowden N S and Merrill C 2014 *Technology and Engineering Teacher* **73** 30–35 (available at: www.proquest.com/scholarly-journals/3d-printing-technology-engineering-education/docview/1524958383/se-2)
[7] Liu C, Qin H and Mather P 2007 *J. Mater. Chem.* **17** 1543–58
[8] Mehrpouya M, Vahabi H, Janbaz S, Darafsheh A, Mazur T R and Ramakrishna S 2021 *Polymer* **230** 124080
[9] Akbar I, El Hadrouz M, El Mansori M and Lagoudas D 2022 *Eur. Polym. J.* **168** 111106
[10] Vatanparast S, Boschetto A, Bottini L and Gaudenzi P 2023 *Appl. Sci.* **13** 7744
[11] Ge Q, Qi H J and Dunn M L 2013 *Appl. Phys. Lett.* **103** 131901
[12] Momeni F, Mehdi Hassani N S M, Liu X and Ni J 2017 *Mater. Des.* **122** 42–79
[13] Ahmed A, Arya S, Gupta V, Furukawa H and Khosla A 2021 *Polymer* **228** 123926
[14] Chu H, Yang W, Sun L, Cai S, Yang R, Liang W, Yu H and Liu L 2020 *Micromachines* **11** 796
[15] Khalid M Y, Arif Z U and Ahmed W 2022 *Macromol. Mater. Eng.* **307** 2200003
[16] Yuan C, Lu T and Wang T 2022 *Forces Mech.* **7** 100081
[17] Khalid M Y, Arif Z U, Noroozi R, Zolfagharian A and Bodaghi M 2022 *J. Manuf. Process.* **81** 759–97
[18] Alshebly Y S, Nafea M, Ali M S M and Almurib H A F 2021 *Eur. Polym. J.* **159** 110708
[19] Pei E and Loh G H 2018 *Prog. Addit. Manuf.* **3** 95–107
[20] Miao S *et al* 2017 *Mater. Today* **20** 577–91
[21] Li Y, Zhang F, Liu Y and Leng J 2020 *Sci. China Technol. Sci.* **63** 545–60
[22] Chen X, Han S, Wu W, Wu Z, Yuan Y, Wu J and Liu C 2022 *Small* **18** 2106824
[23] Javaid M and Haleem A 2019 *Clin. Epidemiol. Glob. Health* **7** 317–21
[24] Kalogeropoulou M, Díaz-Payno P J, Mirzaali M J, van Osch G J V M, Fratila-Apachitei L E and Zadpoor A A 2024 *Biofabrication* **16** 022002
[25] Thakur V, Singh R, Kumar R and Gehlot A 2022 *Int. J. Interact. Des. Manuf.* **17** 1–20
[26] Kuang X, Roach D J, Wu J, Hamel C M, Ding Z, Wang T, Dunn M L and Qi H J 2019 *Adv. Funct. Mater.* **29** 1805290

[27] Isaac C W and Duddeck F 2023 *Virtual Phys. Prototyp.* **18** e2197436
[28] Bodaghi M, Damanpack A and Liao W 2017 *Mater. Des.* **135** 26–36
[29] Champeau M, Heinze D A, Viana T N, de Souza E R, Chinellato A C and Titotto S 2020 *Adv. Funct. Mater.* **30** 1910606
[30] Subeshan B, Baddam Y and Asmatulu E 2021 *Prog. Addit. Manuf.* **6** 495–516
[31] Ehrmann G and Ehrmann A 2021 *J. Appl. Polym. Sci.* **138** 50847
[32] Peng B, Yang Y and Cavicchi K A 2020 *Multifunct. Mater.* **3** 042002
[33] Rastogi P and Kandasubramanian B 2019 *Chem. Eng. J.* **366** 264–304
[34] Guo S, Cui H, Agarwal T and Zhang L G 2024 *Small* e2307750
[35] Korrayi R R, Jena A, Marupalli B C, Samal B B, Varshney S K and Kumar C S 2024 *Additive Manufacturing With Novel Materials: Processes, Properties and Applications* (Wiley Online Library) pp 429–57
[36] Mishra A and Behera A 2023 *Int. J. Interact. Des. Manuf.* 1–31
[37] Hamidi N, Abdullah J, Shuib R K, Aziz I and Namazi H 2024 *Eng. Res. Express* **6** 012402
[38] Tezerjani S M D, Yazdi M S and Hosseinzadeh M H 2022 *Mater. Today Commun.* **33** 104262
[39] Li J, Liang Z, Liu J, Yu C, Zhang X and Kan Q 2023 *Smart Mater. Struct.* **32** 035030
[40] Zhao J, Han M and Li L 2021 *Mater. Des.* **203** 109617
[41] Garzon-Hernandez S, Arias A and Garcia-Gonzalez D 2020 *Composites* B **201** 108373
[42] Hu G, Damanpack A, Bodaghi M and Liao W H 2017 *Smart Mater. Struct.* **26** 125023
[43] Baniasadi M, Yarali E, Bodaghi M, Zolfagharian A and Baghani M 2021 *Int. J. Mech. Sci.* **192** 106082
[44] Bodaghi M, Damanpack A and Liao W 2016 *Smart Mater. Struct.* **25** 105034
[45] Bodaghi M, Damanpack A and Liao W 2018 *Smart Mater. Struct.* **27** 065010
[46] Yang G H, Yeo M, Koo Y W and Kim G H 2019 *Macromol. Biosci.* **19** 1800441
[47] Kouka M A, Abbassi F, Habibi M, Chabert F, Zghal A and Garnier C 2023 *Adv. Eng. Mater.* **25** 2200650
[48] Tobushi H, Hashimoto T, Hayashi S and Yamada E 1997 *J. Intell. Mater. Syst. Struct.* **8** 711–8
[49] Liu Y, Gall K, Dunn M L, Greenberg A R and Diani J 2006 *Int. J. Plast.* **22** 279–313
[50] Shojaei A, Xu W, Yan C, Yang Q and Li G 2022 *Front. Mech. Eng.* **8** 956129
[51] Yarali E, Taheri A and Baghani M 2020 *J. Intell. Mater. Syst. Struct.* **31** 1243–83
[52] Huang R, Zheng S, Liu Z and Ng T Y 2020 *Int. J. Appl. Mech.* **12** 2050014
[53] Nguyen T D 2013 *Polym. Rev.* **53** 130–52
[54] Yan C and Li G 2022 *J. Appl. Phys.* **131** 111101
[55] Pivar M, Gregor-Svetec D and Muck D 2021 *Polymers* **14** 117
[56] Popescu D, Zapciu A, Amza C, Baciu F and Marinescu R 2018 *Polym. Test.* **69** 157–66
[57] Ansaripour A, Heidari-Rarani M, Mahshid R and Bodaghi M 2024 *Int. J. Adv. Manuf. Technol.* **132** 1–16
[58] Nezhad I S, Golzar M, Behravesh A H and Zare S 2022 *Int. J. Adv. Manuf. Technol.* **120** 959–74
[59] Ngo T D, Kashani A, Imbalzano G, Nguyen K T and Hui D 2018 *Composites* B **143** 172–96
[60] Li Y, Guo S-S, He Y and Liu Z 2015 *Int. J. Comput. Mater. Sci. Eng.* **4** 1550001
[61] Diani J, Liu Y and Gall K 2006 *Polym. Eng. Sci.* **46** 486–92
[62] Morshedian J, Khonakdar H A and Rasouli S 2005 *Macromol. Theory. Simul.* **14** 428–34
[63] Zhao W, Zhang F, Leng J and Liu Y 2019 *Compos. Sci. Technol.* **184** 107866
[64] Wan M, Yu K and Sun H 2022 *Compos. Struct.* **279** 114791
[65] Arruda E M and Boyce M C 1993 *J. Mech. Phys. Solids* **41** 389–412
[66] Liu T, Liu L, Zeng C, Liu Y and Leng J 2020 *Compos. Sci. Technol.* **186** 107935
[67] Han M, Yang Y and Li L 2020 *Addit. Manuf.* **34** 101223
[68] Reese S, Böl M and Christ D 2010 *Comput. Methods Appl. Mech. Eng.* **199** 1276–86
[69] Long K N, Dunn M L and Qi H J 2010 *Int. J. Plast.* **26** 603–16
[70] Xu W and Li G 2010 *Int. J. Solids Struct.* **47** 1306–16
[71] Li Y, Hu J and Liu Z 2017 *Int. J. Solids Struct.* **124** 252–63
[72] Domingo-Espin M, Puigoriol-Forcada J M, Garcia-Granada A-A, Llumà J, Borros S and Reyes G 2015 *Mater. Des.* **83** 670–7
[73] Zou R, Xia Y, Liu S, Hu P, Hou W, Hu Q and Shan C 2016 *Composites* B **99** 506–13
[74] Alaimo G, Marconi S, Costato L and Auricchio F 2017 *Composites* B **113** 371–80
[75] Somireddy M, Czekanski A and Singh C V 2018 *Mater. Today Commun.* **15** 143–52
[76] Hou Z, Tian X, Zheng Z, Zhang J, Zhe L, Li D, Malakhov A V and Polilov A N 2020 *Composites* B **189** 107893
[77] Kim J H, Kang T J and Yu W-R 2010 *Int. J. Plast.* **26** 204–18
[78] Guo X, Liu L, Liu Y, Zhou B and Leng J 2014 *Smart Mater. Struct.* **23** 105019
[79] Hu G, Damanpack A, Bodaghi M and Liao W 2017 *Smart Materials, Adaptive Structures and Intelligent Systems* (Snowbird, Utah, USA, *18–20 September)* vol 1 (The American Society of Mechanical Engineers) p V001T08A003
[80] Bodaghi M and Liao W 2019 *Smart Mater. Struct.* **28** 045019
[81] Guo Z, Caner F, Peng X and Moran B 2008 *J. Mech. Phys. Solids* **56** 2338–57
[82] Li M and Sun B-H 2023 *J. Appl. Mech.* **90** 091004
[83] Gurson A L 1977 *J. Eng. Mater. Technol.* **99** 2–15
[84] Valizadeh I and Weeger O 2022 *Int. J. Mech. Sci.* **226** 107335
[85] Momeni F and Ni J 2020 *Engineering* **6** 1035–55
[86] Zhang Z, Demir K G and Gu G X 2019 *Int. J. Smart Nano Mater.* **10** 205–24
[87] Timoshenko S 1925 *J. Opt. Soc. Am.* **11** 233–55
[88] Sydney Gladman A, Matsumoto E A, Nuzzo R G, Mahadevan L and Lewis J A 2016 *Nat. Mater.* **15** 413–8
[89] Raviv D *et al* 2014 *Sci. Rep.* **4** 7422
[90] Deng D and Chen Y 2015 *J. Mech. Des.* **137** 021701
[91] Teoh J, An J, Chua C, Lv M, Krishnasamy V and Liu Y 2017 *Virtual Phys. Prototyp.* **12** 61–68
[92] Wang Q, Tian X, Huang L, Li D, Malakhov A V and Polilov A N 2018 *Mater. Des.* **155** 404–13
[93] Odent J, Vanderstappen S, Toncheva A, Pichon E, Wallin T J, Wang K, Shepherd R F, Dubois P and Raquez J-M 2019 *J. Mater. Chem.* A **7** 15395–403
[94] Zeng S, Feng Y, Gao Y, Tan J and Wei Z 2021 4D printed bilayer helical structures mechanical behaviors and shape memory effects *Smart Materials, Adaptive Structures and Intelligent Systems* (*Virtual, Online, 14–15 September)* (The American Society of Mechanical Engineers) p V001T07A008
[95] Moosabeiki V *et al* 2024 *Commun. Mater.* **5** 10
[96] Ge Q, Dunn C K, Qi H J and Dunn M L 2014 *Smart Mater. Struct.* **23** 094007

[97] Wu J, Yuan C, Ding Z, Isakov M, Mao Y, Wang T, Dunn M L and Qi H J 2016 *Sci. Rep.* **6** 24224
[98] Wang W, Yu C Y, Serrano P A A and Ahn S-H 2019 *Composites* B **164** 198–204
[99] Zhang Q, Zhang K and Hu G 2016 *Sci. Rep.* **6** 22431
[100] Su J-W, Tao X, Deng H, Zhang C, Jiang S, Lin Y and Lin J 2018 *Soft Matter* **14** 765–72
[101] Guo W, Li M and Zhou J 2013 *Smart Mater. Struct.* **22** 115028
[102] Armon S, Efrati E, Kupferman R and Sharon E 2011 *Science* **333** 1726–30
[103] Aharoni H, Sharon E and Kupferman R 2014 *Phys. Rev. Lett.* **113** 257801
[104] Stroganov V, Pant J, Stoychev G, Janke A, Jehnichen D, Fery A, Handa H and Ionov L 2018 *Adv. Funct. Mater.* **28** 1706248
[105] Zakharchenko S, Puretskiy N, Stoychev G, Waurisch C, Hickey S G, Eychmüller A, Sommer J-U and Ionov L 2013 *J. Mater. Chem.* B **1** 1786–93
[106] Yuan C, Ding Z, Wang T, Dunn M L and Qi H J 2017 *Smart Mater. Struct.* **26** 105027
[107] Westbrook K K, Kao P H, Castro F, Ding Y and Qi H J 2011 *Mech. Mater.* **43** 853–69
[108] Yu K, Ge Q and Qi H J 2014 *Nat. Commun.* **5** 3066
[109] Momeni F, Sabzpoushan S, Valizadeh R, Morad M R, Liu X and Ni J 2019 *Renew. Energy* **130** 329–51
[110] Zhang Q, Yan D, Zhang K and Hu G 2015 *Sci. Rep.* **5** 8936
[111] Boley J W, Van Rees W M, Lissandrello C, Horenstein M N, Truby R L, Kotikian A, Lewis J A and Mahadevan L 2019 *Proc. Natl Acad. Sci.* **116** 20856–62
[112] Aharoni H, Xia Y, Zhang X, Kamien R D and Yang S 2018 *Proc. Natl Acad. Sci.* **115** 7206–11
[113] Ji Z, Yan C, Yu B, Zhang X, Cai M, Jia X, Wang X and Zhou F 2019 *Adv. Mater. Technol.* **4** 1800713
[114] Lee A Y, An J and Chua C K 2017 *Engineering* **3** 663–74
[115] Lee A Y, An J, Chua C K and Zhang Y 2019 *Engineering* **5** 1159–70
[116] Ding Z, Yuan C, Peng X, Wang T, Qi H J and Dunn M L 2017 *Sci. Adv.* **3** e1602890
[117] Feng Y, Xu J, Zeng S, Gao Y and Tan J 2020 *Smart Mater. Struct.* **29** 085042
[118] Feng Y, Yan W, Qiu H, Hong Z, Zeng S, Xu J, Cui K and Tan J 2022 *Smart Mater. Struct.* **31** 085001
[119] Lu H, Wang X, Yao Y and Fu Y Q 2018 *Smart Mater. Struct.* **27** 065023
[120] Helfrich W 1986 *J. Chem. Phys.* **85** 1085–7
[121] Feng Y, Zeng S, Gao Y, Zheng H, Qiu H and Tan J 2019 Design and realization of temperature-driven smart structure based on shape memory polymer in 4D printing *Smart Materials, Adaptive Structures and Intelligent Systems* vol 59131 (American Society of Mechanical Engineers) p V001T04A002
[122] Zeng S, Gao Y, Feng Y, Zheng H, Qiu H and Tan J 2019 *Smart Mater. Struct.* **28** 105031
[123] Dano M-L and Hyer M W 1998 *Int. J. Solids Struct.* **35** 2101–20
[124] Deshpande V, Myers O, Fadel G and Li S 2021 *Smart Materials, Adaptive Structures and Intelligent Systems* (*Virtual, Online, 14–15 September*) (The American Society of Mechanical Engineers) p V001T07A010
[125] Song J, Feng Y, Wang Y, Zeng S, Hong Z, Qiu H and Tan J 2021 *Appl. Math. Mech.* **42** 1619–32
[126] Bartels S, Bonito A and Nochetto R H 2017 *Commun. Pure Appl. Math.* **70** 547–89
[127] Bartels S, Bonito A, Muliana A H and Nochetto R H 2018 *J. Comput. Phys.* **354** 512–28
[128] Liu Z, Liu H, Duan G and Tan J 2020 *Math. Mech. Solids* **25** 348–61
[129] van Rees W M, Matsumoto E A, Gladman A S, Lewis J A and Mahadevan L 2018 *Soft Matter* **14** 8771–9
[130] Kappel E, Stefaniak D, Holzhüter D, Hühne C and Sinapius M 2013 *Composites* A **51** 89–98
[131] Thölking H, Cerbe F and Sinapius M 2023 *Mater. Today Proc.* (https://doi.org/10.1016/j.matpr.2023.02.040)
[132] Manikandan N and Rajesh P 2023 *Prog. Addit. Manuf.* **9** 1–9
[133] Tibbits S 2014 *Archit. Des.* **84** 116–21
[134] Qi X, Chen G, Li Y, Cheng X and Li C 2019 *Engineering* **5** 721–9
[135] Wang C, Tan X P, Tor S B and Lim C 2020 *Addit. Manuf.* **36** 101538
[136] Liu R, Liu S and Zhang X 2021 *Int. J. Adv. Manuf. Technol.* **113** 1943–58
[137] Ko H, Lu Y, Yang Z, Ndiaye N Y and Witherell P 2023 *J. Manuf. Syst.* **67** 213–28
[138] Sossou G, Demoly F, Belkebir H, Qi H J, Gomes S and Montavon G 2019 *Mater. Des.* **181** 108074
[139] Sossou G, Demoly F, Belkebir H, Qi H J, Gomes S and Montavon G 2019 *Mater. Des.* **175** 107798
[140] Sossou G, Demoly F, Montavon G and Gomes S 2018 *Proc. CIRP* **70** 120–5
[141] Chinchanikar S and Shaikh A A 2022 *J. Mater. Eng. Perform.* **31** 6112–30
[142] Jin Z, Zhang Z, Demir K and Gu G X 2020 *Matter* **3** 1541–56
[143] Meng L, McWilliams B, Jarosinski W, Park H-Y, Jung Y-G, Lee J and Zhang J 2020 *JOM* **72** 2363–77
[144] Ng W L, Goh G L, Goh G D, Ten J S J and Yeong W Y 2024 *Adv. Mater.* 2310006
[145] Liu X, Tian S, Tao F and Yu W 2021 *Composites* B **224** 109152
[146] Yan C, Feng X, Wick C, Peters A and Li G 2021 *Polymer* **214** 123351
[147] Yan C, Feng X and Li G 2021 *ACS Appl. Mater. Interfaces* **13** 60508–21
[148] Rosales C A G, Rahman M F, Xu H and Tseng T L B 2021 *4th European Int. Conf. on Industrial Engineering and Operations Management* (*Rome, Italy,* 2–5 *August)* (available at: www.ieomsociety.org/rome2020/proceedings/)
[149] Gunes S, Ulkir O and Kuncan M 2024 *J. Polym. Sci.* **62** 1864–89
[150] Goswami S, Ghosh R, Neog A and Das B 2021 *Mater. Today Proc.* **46** 5838–43
[151] Sun X, Zhou K, Demoly F, Zhao R R and Qi H J 2024 *J. Appl. Mech.* **91** 030801
[152] Hamel C M, Roach D J, Long K N, Demoly F, Dunn M L and Qi H J 2019 *Smart Mater. Struct.* **28** 065005
[153] Su J-W, Li D, Xie Y, Zhou T, Gao W, Deng H, Xin M and Lin J 2020 *Smart Mater. Struct.* **30** 015028
[154] Wang J, Zhu B, Hui C-Y and Zehnder A T 2023 *J. Mech. Phys. Solids* **177** 105324
[155] Jordan B, Gorji M B and Mohr D 2020 *Int. J. Plast.* **135** 102811
[156] Ibarra D S, Mathews J, Li F, Lu H, Li G and Chen J 2022 *Polymer* **261** 125395
[157] Lockett F 1965 *Int. J. Eng. Sci.* **3** 59–75
[158] Simo J C 1987 *Comput. Methods Appl. Mech. Eng.* **60** 153–73
[159] Kalina K A, Linden L, Brummund J and Kästner M 2023 *Comput. Mech.* **71** 827–51
[160] Fernández M, Rezaei S, Rezaei Mianroodi J, Fritzen F and Reese S 2020 *Adv. Model. Simul. Eng. Sci.* **7** 1–27
[161] Fernández M, Fritzen F and Weeger O 2022 *Int. J. Numer. Methods Eng.* **123** 577–609
[162] Oeser M and Freitag S 2009 *Int. J. Numer. Methods Eng.* **78** 843–62

[163] Freitag S, Graf W and Kaliske M 2013 *Comput. Struct.* **124** 29–37
[164] Zopf C and Kaliske M 2017 *Comput. Struct.* **182** 504–25
[165] Linka K, Hillgärtner M, Abdolazizi K P, Aydin R C, Itskov M and Cyron C J 2021 *J. Comput. Phys.* **429** 110010
[166] Abdolazizi K P, Linka K and Cyron C J 2023 arXiv:2303.12164
[167] Latorre M and Montáns F J 2015 *Comput. Mech.* **56** 503–31
[168] Succi S and Coveney P V 2019 *Phil. Trans. R. Soc.* A **377** 20180145
[169] Gao X, Qi S, Kuang X, Su Y, Li J and Wang D 2021 *Addit. Manuf.* **37** 101658
[170] Lalegani Dezaki M and Bodaghi M 2023 *Int. J. Adv. Manuf. Technol.* **126** 35–48